PERGAMON

Journal of Atmospheric and Solar-Terrestrial Physics 63 (2001) 771–780

Journal of ATMOSPHERIC AND SOLAR-TERRESTRIAL PHYSICS

www.elsevier.nl/locate/jastp

Modelling of particle charging in the polar summer mesosphere: Part 2—Application to measurements

Franz-Josef Lübken*, Markus Rapp

Leibniz Institut für Atmosphärenphysik, Schlosstr. 6, 18225 Kühlungsborn, Germany

Received 26 February 2000; accepted 22 November 2000

Abstract

A model describing the charging of aerosol particles in the vicinity of the polar summer mesosphere is applied to in situ measurements of electron and ion number densities. More general results from this model are presented in a companion paper (Rapp and Lübken, 2001). Here we apply this model to various in situ measurements. Charging of the aerosols causes disturbances in the electron and ion number density profiles which depend on various parameters, such as the electron/ion production rate Q, the electron/ion recombination coefficient α, the aerosol size, r_A, and the aerosol number density N_A. We have analyzed measurements from rocket flights where at least two of these parameters are known (in most cases Q and α). Under most circumstances the disturbance in the electron density profile Δn_e ('biteout') depends on r_A and N_A in a different way than the disturbance in the positive ion density profile Δn_i. In many cases this allows to unambiguously determine r_A and N_A from measurements of Δn_e and Δn_i. From a total of 11 flights found in the literature we have analyzed in detail four cases which are characterized by simultaneous observations of noctilucent clouds (NLC) and/or polar mesosphere summer echoes (PMSE) by ground based or in situ techniques. In all cases our model successfully explains the observed plasma disturbances in terms of aerosol charging. During NLC conditions we arrive at particle radii of 32–60 nm and number densities of 110–850 cm^{-3}. Assuming that the particles consist of water ice the amount of ice in the particles corresponds to gas phase water vapor concentrations of 4–14 ppm_v which is rather large compared to 'standard' model values. These large values support the idea that water vapor is collected by the aerosols in a larger horizontal area and/or extended altitude range when they sediment from the mesopause region (88 km) to typical NLC altitudes (82 km). In one flight we arrive at much smaller (1 nm) and much more abundant (several 100,000 cm^{-3}) aerosol particles.

Keywords: Polar summer mesosphere; Aerosol particles; Charging processes; D-region; PMSE; NLC

1. Introduction

The lower ionosphere at polar latitudes is sometimes significantly modified by the presence of aerosol particles which exist at the very low temperatures of the upper mesosphere during summer. These aerosols presumably consist of water ice and may cause a depletion in the electron and ion density profile since these plasma species may be captured by the aerosols. It could also happen that an ion enhancement is created in case that the ion density is determined by the recombination with electrons (i.e., the ion/electron recombination rate is large in comparison with the ion/aerosol recombination rate) but the electron density is depleted. A more quantitative and complete description of the effect of aerosols on the mean background plasma density requires a careful consideration of all charging mechanisms involved and a detailed calculation of the charge fluxes between the plasma environment and the aerosols. Based on previous work by Parthasarathy (1976), Reid (1990), and Jensen and Thomas (1991) we have developed such a model which takes into account these processes. The physical mechanisms involved and details of the models are described in a companion paper by Rapp and Lübken (2001) (hereafter R&L). In that paper we

* Corresponding author. Tel.: +49-38293-68100; fax: +49-38293-6850.

E-mail address: luebken@iap-kborn.de (F.-J. Lübken).

1364-6826/01/$ - see front matter
PII: S1364-6826(01)00007-4

discuss in detail some general results of particle charging in the upper mesosphere during summer and in particular the importance of the background ionization and the recombination coefficient on the plasma disturbance. In this paper we apply this model to actual measurements performed by rocket-borne instrumentation during the last 34 years.

In general, the measurement of a single species alone does not allow to make any significant statement about the aerosol particles since there are too many combinations of aerosol and plasma parameters which can explain a given disturbance. We will therefore concentrate on those rocket flights where at least two independent species have been measured (e.g. electron and positive ion densities). We will only briefly discuss the measurements which indicate that the aerosol particles could have been positively charged due to photoemission (if the aerosol particles consist of pure water ice they cannot be positively charged since the work function is too high to allow for photoemission by solar radiation). This specific aspect of particle charging is presented elsewhere (see e.g., Havnes et al., 1996; Rapp and Lübken, 1999).

Apart from in situ measurements the aerosols in the mesosphere may eventually be seen from the ground by the naked eye or by lidars, a phenomenon known as 'noctilucent clouds' (NLC). Furthermore, these aerosols are believed to be involved in the creation of very intense radar backscatter echoes called 'polar mesosphere summer echoes' (PMSE). Reviews on NLC and PMSE observations and theories including a comprehensive discussion on the role of aerosol particles creating these phenomena have been published in the literature (Gadsden and Schröder 1989; Cho and Röttger, 1997).

In the following section we briefly summarize the existing data base regarding in situ measurements of plasma parameters in the vicinity of NLC and PMSE. In Section 3 we apply our model to four sets of measurements. We will present in detail the results from our model and the implications for the aerosol particle properties. Finally, we discuss and summarize the results in Section 4.

2. Simultaneous measurements of electron and ion number densities

A survey of simultaneous measurements of plasma density profiles published in the literature shows that there have been only 11 flights during which electron and ion number densities have been measured together with simultaneous observations of NLC and/or PMSE (see Table 1). In addition, there have been two flights where electron densities were measured simultaneously with aerosol charge densities (flights ECT02, ECT07, see Table 1). For these flights we have determined the ion number density using the condition of local charge neutrality. In all cases we apply our model to the electron and ion density disturbance at altitudes where the effect is largest. The undisturbed electron and ion densities, N_e and N_i, respectively, have also been deduced from the measurements by interpolating the profiles from above and below the disturbed regions. They are related to the electron/ion recombination coefficient α and the mean production rate Q by

$$N_e = N_i = \sqrt{Q/\alpha}. \tag{1}$$

We will later show model results of relative electron and positive ion disturbances, Δn_e and Δn_i, as a function of particle number density and particle radius, N_A and r_A, respectively. Δn_e and Δn_i are defined as

$$\Delta n_e = 100\frac{n_e - N_e}{N_e}, \quad \Delta n_i = 100\frac{n_i - N_i}{N_i}, \tag{2}$$

where n_e (n_i) is the free electron (positive ion) number density in the presence of aerosol particles and $N_e = N_i = \sqrt{Q/\alpha}$ are the undisturbed background number densities which would be there if no particles were present. A value of $\Delta n_e = -100\%$ implies that all electrons have been captured by the aerosol particles, $\Delta n_e = 0\%$ describes no disturbance at all. A positive percentage stands for an enhancement.

It turns out that one of the most critical parameters in the model is the electron/ion recombination coefficient α which depends on the ion composition (see R&L for more details). We have determined α from measurements of positive ion composition if such measurements are available (see Table 1). In cases of a deep ion density biteout (i.e., if basically no ions are left in the disturbed region) we have taken the positive ion composition from directly above the disturbance. The (effective) recombination coefficient is determined by the ion composition through

$$\alpha = \frac{1}{n_i}\sum_j \alpha_j (n_i)_j, \tag{3}$$

where n_i is the total positive ion number density and α_j and $(n_i)_j$ are the recombination coefficient and the number density of the jth ion species. From the undisturbed plasma density $N_{e,i}$ and α we then determine the electron and ion production rate $Q = \alpha N_{e,i}^2$.

We have investigated whether or not a NLC and/or PMSE was detected during the rocket flight (see Table 2) and have used this information to classify the cases as 'NLC' and/or 'PMSE'. The data base described above has been sorted according to the following scenarios:

Case 1. A significant electron biteout is observed together with basically no disturbance in the ion number density profile. The electron biteout is located ...

(a) ... inside a NLC layer (flights S26/1 and CAMP/P)
(b) ... inside a PMSE layer (flights TURBO-B and ECT02)

Case 2. A deep depletion both in the electron and ion number density profiles is observed ...

(a) ... inside a NLC (flight DECA93)
(b) ... in the PMSE altitude region (flights P69, JK72, and SCT06)

Table 1
Rocket flights with simultaneous measurements of electron and positive ion number density during NLC and/or PMSE events (Rel. Instr. = relevant Instruments: instruments used to measure electrons and positive ions, Fa = Faraday Rotation experiment, EEP = Electrostatic electron probe, EIP = Electrostatic positive ion probe, MS = Mass spectrometer, PD = Particle detector)

Flight	Date	Time	Launch site	Rel. Instr.	Reference
P69	26.06.66	21:47UT	Andøya	Fa, EIP	Pedersen et al. (1969)
JK72	08.08.71	12:11UT	Andøya	Fa, MS, EIP	Johannessen and Krankowsky (1972) Johannessen et al. (1972)
S26/1	30.07.78	23:33UT	Kiruna	Fa, MS, EIP	Björn et al. (1985), Kopp et al. (1985)
S26/2	12.08.78	23:38UT	Kiruna	Fa, MS	Kopp et al. (1985)
CAMP/P	03.08.82	23:32UT	Kiruna	Fa, MS	Koppet al. (1984)
DECA91	09.08.91	23:15UT	Kiruna	Fa, MS, EIP	Wälchli et al. (1993), Goldberg et al. (1993), Balsiger et al. (1993), Friedrich et al. (1994)
TURBOA	09.08.91	23:15UT	Kiruna	EIP, EEP	Blix and Thrane (1993), Friedrich et al. (1994)
TURBOB	01.08.91	01:40UT	Kiruna	EIP, EEP	Lübken et al. (1993)
DECA93	02.08.93	00:23UT	Kiruna	Fa, MS	Balsiger et al. (1996), Gumbel and Witt (1998)
DECB93	02.08.93	01:02UT	Kiruna	Fa, EIP	Blix (1999), Gumbel and Witt (1998)
SCT06	01.08.93	01:46UT	Andøya	EIP, EEP	Blix (1999)
ECT02	28.07.94	22:39UT	Andøya	EEP, PD	Havnes et al. (1996), Lübken et al. (1998)
ECT07	31.07.94	00:50UT	Andøya	EEP, PD	Havnes et al. (1996), Rapp and Lübken (1999)

Table 2
Plasma parameters measured at altitudes where disturbances are observed for the flights summarized in Table 1. (u) = upleg, (d) = downleg, a.u. = arbitrary units

Flight	z_{dist} (km)	$\sqrt{\frac{Q}{\alpha}}$ (cm^{-3})	n_e (cm^{-3})	n_i (cm^{-3})	most. ab. ion	α (cm^3/s)	Q ($cm^{-3}\,s^{-1}$)	NLC (km)	PMSE (km)
P69	87	9000	400	3300				No	
JK72	85.2	13 500	3500	4000	$H^+(H_2O)_2$	2.1×10^{-6}	383		
S26/1	83	440	45	440	$H^+(H_2O)_5$	7.0×10^{-6}	1.35	83 ± 1	
S26/2	87	4000	4000	2500	O_2^+	3.7×10^{-6}	58	No	
CAMP/P	83	30 000	8000	30 000	$H^+(H_2O)_4$	7.0×10^{-6}	6300	83 ± 1	
DECA91	83.2	1000	1000	3000	$H^+(H_2O)_4$	6.9×10^{-6}	6.9	83 ± 0.5	83.8
TURBOA	83(u)	4.0 nA		6.4 nA				83 ± 0.5	83.8
	83(d)	1 (a.u.)	4 (a.u.)	1.6 (a.u.)					
TURBOB	84.5	10 000	2000	10 000				No	84–86
DECA93	83	30	~0	2.0	$H^+(H_2O)_4$	6.9×10^{-6}	0.006	83–84	No
DECB93	83	105	20	240				83–84	No
SCT06	85.2(u)	6000	~0	2500				No	85–87
	85(d)	11 000	~0	~0				No	85–87
ECT02	85.5	4000	~0	4000				No	85–90
ECT07	83	3000	6000	~0				83	82–88

Case 3. A significant ion number density enhancement is measured inside a NLC layer ...

(a) ... together with a deep electron biteout (flight DECB93)
(b) ... together with an unknown electron profile (flight DECA91 at 83.2 km, and flight TURBOA)

Case 4. An enhancement of electron number densities is detected inside a NLC layer but the ion profile is not known (flights TURBOA and ECT07).

We note that in flights DECA91 and TURBOA (Case 3b) a PMSE layer was also present but above the NLC layer, i.e., not at the altitudes of prime interest here. For flight ECT07 both layers, i.e., NLC and PMSE were present at the same altitude. We still label this case as 'NLC' since the particle size was estimated to be 30 nm (Rapp and Lübken, 1999). In our classification these particles are 'large' and are therefore typical for NLC conditions.

It is evident from this list that plasma disturbances occur in a great variety of cases: electron biteouts are observed with all three cases of ion density disturbances (unmodified, depletion, and enhancement).

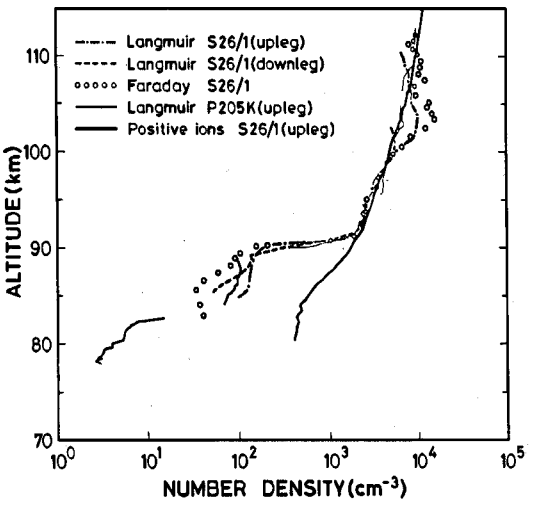

Fig. 1. Plasma density measurements during flight S26/1. The thick solid line shows the hardly disturbed positive ion profile measured on the ascent of the trajectory and the other data points show results of the electron number density measurements. This figure has been taken from Björn et al. (1985), copyright by the American Geophysical Union.

3. Model analysis of four cases of plasma disturbances

We will now interpret the observations summarized above by means of our aerosol charging model. As we have shown in R&L the production rate Q and the recombination coefficient α need to be known to unambiguously analyze the measurements in terms of aerosol charging and to determine aerosol parameters from the plasma measurements. We will therefore only analyze flights where the recombination coefficient is known from mass spectrometric measurements and the production rate is given by $Q = \alpha N_e^2$. Since the charging mechanism depends only slightly on temperature we have used mean summer temperatures from Lübken (1999) in our model calculations.

We concentrate on four flights: S26/1 as being representative for case 1a, DECA93 for case 2a, JK72 for case 2b, and finally DECB93 for case 3a. Case 4 is special since electron density enhancements cannot be explained by aerosol charging as presented so far but require an additional source of electrons presumably by photo emission of electrons from particles (see R&L for more details). This in turn requires the work-function of the aerosols to be reduced in comparison with water ice. Model calculations on this topic and applications to measurements are presented in Rapp and Lübken (1999) and will not be repeated here.

3.1. Case 1a (NLC). Flight S26/1

Flight S26/1 is an example of a significant electron biteout together with a more or less undisturbed positive ion number density profile. Fig. 1 shows the original data from Björn et al. (1985). We have applied our model to the plasma density profiles around 83 km which is exactly the altitude where a NLC was observed by rocket-borne photometers (see Fig. 1 in Björn et al., 1985). Note that we attribute the entire disturbance to negatively charged aerosol particles instead of negative ions since negative ions are unlikely to exist at these altitudes during summer conditions (Mitra, 1981; Thomas and Bowman, 1985). Furthermore, we assume that the positive ion profile represents the undisturbed background plasma profile. The ion production rate and recombination coefficient during this flight are then $Q = 1.35\ \mathrm{cm^{-3}\ s^{-1}}$ and $\alpha = 7\times10^{-6}\ \mathrm{cm^3/s}$, respectively (see Table 2). In Fig. 2 model results of electron and ion density disturbances Δn_e and Δn_i are shown as a function of particle radius and aerosol number density for fixed values of Q and α (given above). In addition, we indicate the combinations of r_A and N_A where the amount of water in the aerosol particles corresponds to an atmospheric water vapor mixing ratio of 10 $\mathrm{ppm_v}$.

As can be seen from Fig. 1 an electron depletion of $\Delta n_e \sim 90\%$ was observed during flight S26/1 with basically no disturbance in the ion density profile ($\Delta n_i = 0\%$). The corresponding isolines in Fig. 2 intersect at an aerosol radius of 60 nm and a number density of 180 $\mathrm{cm^{-3}}$. This is an example of an unambiguous determination of the aerosol radius r_A and number density N_A from electron and positive density profiles. How do the numbers stated above vary if we consider instrumental uncertainties which allow the ion density profile to be slightly modified, let's say by up to $\pm 10\%$ from its undisturbed values? From our model we arrive at $r_A = 67$ nm and $N_A = 160\ \mathrm{cm^{-3}}$ for a 10% ion density depletion, and $r_A = 47$ nm and $N_A = 250\ \mathrm{cm^{-3}}$ for a 10% enhancement. We summarize that the mean aerosol radius and number density in the NLC layer at $\sim$83 km during flight S26/1 are $r_A = 60$ nm and $N_A = 180\ \mathrm{cm^{-3}}$, with typical uncertainties of 20% and 40%, respectively.

3.2. Case 2a (NLC). Flight DECA93

Balsiger et al. (1996) reported a very deep biteout in positive ion number densities of $\Delta n_i \sim -90\%$ observed under extremely quiet ionospheric conditions. From their ion composition measurements by a mass spectrometer we derive a recombination coefficient at the upper edge of the biteout of $\alpha = 6.9\times10^{-6}\ \mathrm{cm^3/s}$. Considering a mean total positive ion number density of $N_i \sim 30\ \mathrm{cm^{-3}}$ just above the biteout layer this corresponds to an extremely small mean production coefficient of $Q = \alpha N_i^2 = 0.006\ \mathrm{cm^{-3}s^{-1}}$. Furthermore, the Faraday rotation experiment on board the same rocket detected a complete absence of free electrons in the biteout region (Friedrich, private communication), thus $\Delta n_e = -100\%$. A NLC was observed during the rocket flight by on board photometers (Gumbel and Witt, 1998).

Applying our model to the in situ measurements using the Q and α values stated above results in electron and ion

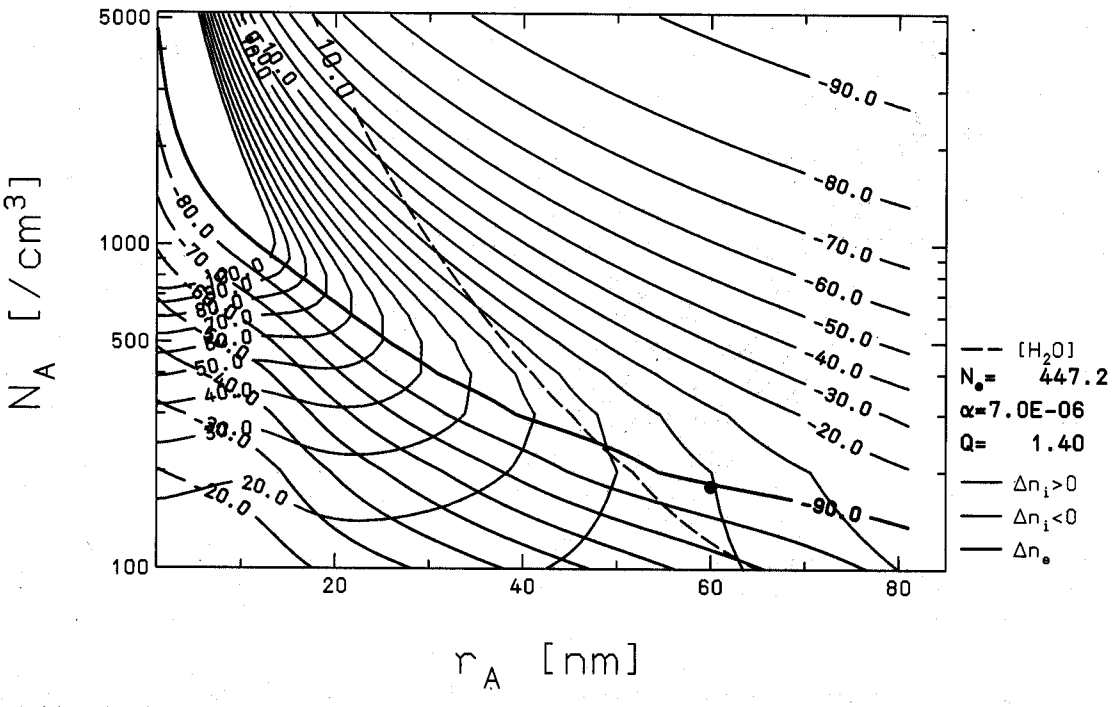

Fig. 2. Model results of relative number density disturbances for electrons (Δn_e, blue lines) and positive ions ($\Delta n_i > 0$, green, and $\Delta n_i < 0$, red lines) as a function of particle radius and number density for the recombination coefficient measured during flight S26/1 by in situ techniques: $\alpha = 7 \times 10^{-6}$ cm^3/s and $Q = 1.4$ cm^{-3} s^{-1} (see Table 2). Δn_e and Δn_i are defined in Section 2. The large dot indicates the intersection of the electron and ion depletion measured during flight S26/1. The violet line shows the combinations of r_A and N_A which would result in a water vapor concentration of 10 ppm$_v$ if the particles evaporated.

depletions as a function of particle radius and number density shown in Fig. 3. It is obvious from this plot that an unambiguous combination of N_A and r_A does not exist since the isolines for $\Delta n_e = -100\%$ and $\Delta n_i = -90\%$ are basically parallel to each other. Thus from the charging model alone we cannot unambiguously determine the aerosol radius and the number density in this case.

Fortunately, there were additional observations on this rocket by a particle impact detector and by a broadband photometer (Gumbel and Witt, 1998). By arguing that the signal of the impact detector is proportional to the mass of the particles (thus to r^3) while the photometer signal is proportional to r^6, altitude profiles of aerosol radius and number densities were obtained. At the NLC and ion biteout altitude (83 km) a mean particle radius of ~52 nm and a number density of approximately 60 particles/cm^3 were determined. From our model we find that this combination should have resulted in electron and ion density depletions of $\Delta n_e = -99\%$ and $\Delta n_i = -46\%$, respectively, the latter being significantly smaller than observed. We note, however, that the quantitative results from the particle detector are somewhat uncertain since the data analysis relies on several unproven assumptions, e.g. that the signal of the impact detector is indeed proportional to r^3. We can therefore speculate about other combinations of N_A and r_A which lead to the same photometer signal (proportional to $N_A r_A^6 = 60 \cdot 52^6 \approx 10^{12}$) but also lead to the observed electron and ion density depletions of $\Delta n_e = -100\%$ and $\Delta n_i = -90\%$. As can be seen from Fig. 3 such a combination indeed exists, namely for a radius of 32 nm and a number density of 850 cm^{-3}. This corresponds to an equivalent water vapor mixing ratio of 10 ppm$_v$. To demonstrate the sensitivity of these results we may assume for a moment a water vapor mixing ratio of 1 ppm$_v$ which would lead to a particle radius of ~8 nm and a number density of ~5000 cm^{-3} (see Fig. 3). This would give a photometer signal more than two orders magnitude smaller than observed.

3.3. *Case 2b. Flight JK72*

We now come to measurements of strong electron and ion depletions in an altitude region where PMSEs are frequently observed (~85 km). We consider the electron and ion number density profile measured during flight JK72 (Johannessen and Krankowsky, 1972) which is reproduced in Fig. 4. Unfortunately, we do not know whether or not a PMSE was present since no radar was available during this flight. As before, we estimate the undisturbed background plasma profile by interpolating the electron and positive ion densities from above and below the disturbed region.

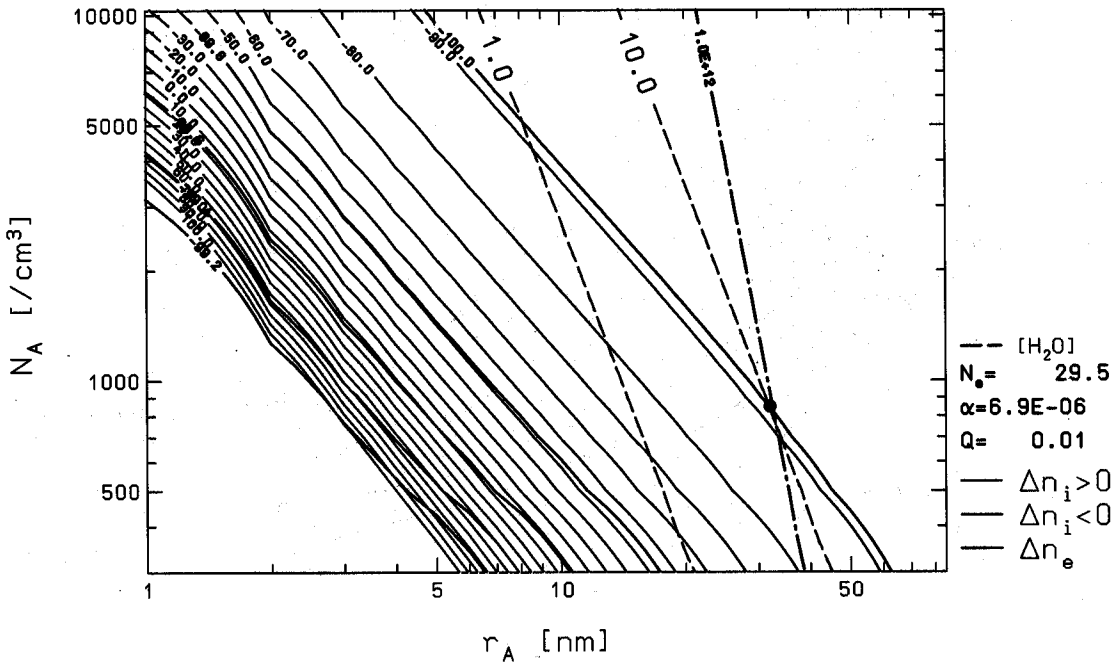

Fig. 3. Model results of relative number density disturbances for electrons (Δn_e, blue lines) and positive ions ($\Delta n_i > 0$, green, and $\Delta n_i < 0$, red lines) as a function of particle radius and number density using the background plasma parameters observed by Balsiger et al. (1996) during flight DECA93 (see Table 2). The violet lines show the combinations of r_A and N_A which would result in a water vapor concentration of 10 and 1 ppm$_v$, respectively, if the particles evaporated. The black dotted-dashed line shows the combinations of r_A and N_A which explain the photometer signal measured on this flight. The black dot indicates the combination of r_A and N_A which explains both the plasma measurements and the photometer observations by Gumbel and Witt (1998).

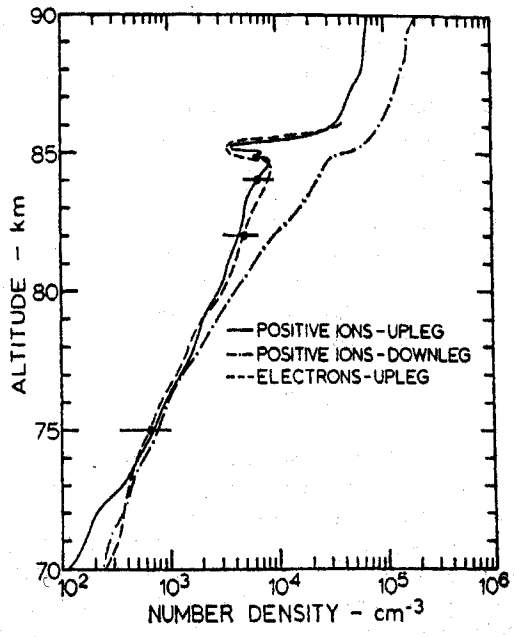

Fig. 4. Electron and ion number densities for flight JK72. This figure has been taken from Johannessen and Krankowsky (1972), copyright by the American Geophysical Union.

During upleg significant depletions in the electron and ion number densites are observed with $\Delta n_e = -75\%$ and $\Delta n_i \sim -70\%$ at an altitude of 85 km. From in situ mass spectrometric measurements of ion composition we derive a recombination coefficient of $\alpha = 2.1 \times 10^{-6}$ cm^3/s. Taking the background ion and electron densities from Fig. 4 this gives a mean production rate of $Q = 383$ cm^{-3} s^{-1}. Our model results for this case are shown in Fig. 5. It is obvious that the observed depletions cannot be reproduced for reasonable values of particle radii and number densities (the $\Delta n_i = -70\%$ and $\Delta n_e = -75\%$ isolines intersect at $r_A = 250$ nm and $N_A = 300$ cm^3 which corresponds to an equivalent water vapor mixing ratio of 1700 ppm$_v$, orders of magnitude larger than standard numbers). The main problem is that the depletion in electrons should be much more pronounced compared to ions due to their higher mobility but the measurements show approximately the same effect both in the electron and ion profiles. We must consider, however, that the electron number densities shown in Fig. 4 have been measured by a Faraday rotation experiment which has an altitude resolution of 1 km only. It could well be that the electron depletion is indeed deeper compared to ions but is not detected due to the poor height resolution of the technique employed during this flight. We will therefore restrict our discussion to the ion

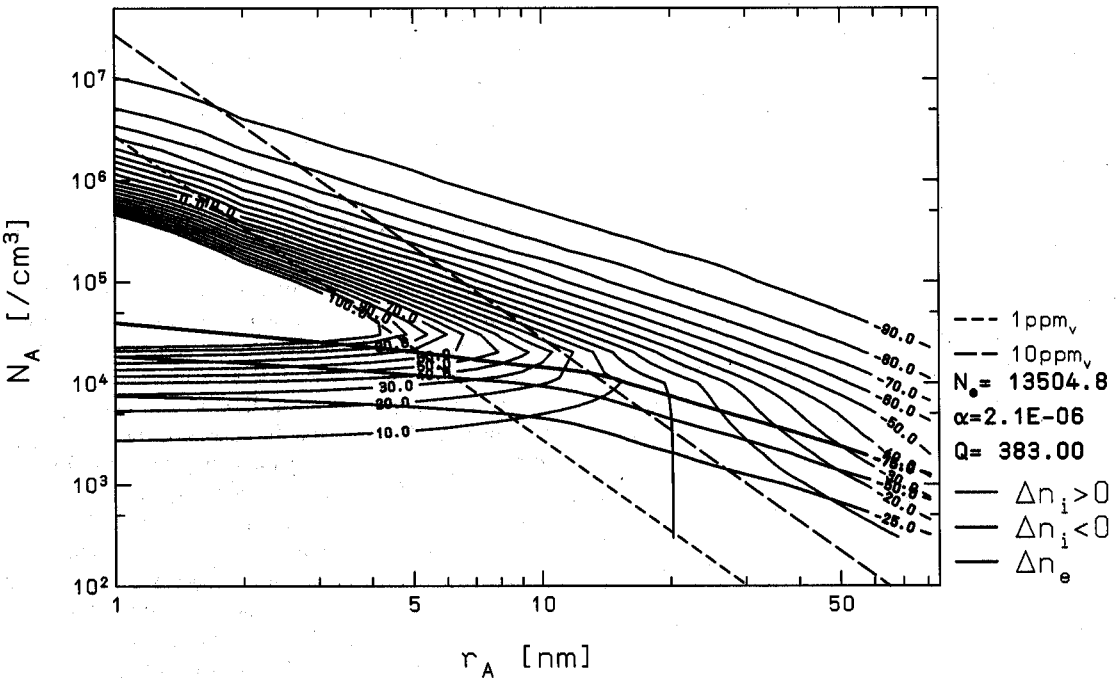

Fig. 5. Model calculations of Δn_e (blue lines) and Δn_i ($\Delta n_i > 0$, green, and $\Delta n_i < 0$, red lines) as a function of particle radius and number density for flight JK72 (see Table 2). The thick dashed lines show the combinations of r_A and N_A which would result in a water vapor concentration of 1 and 10 ppm$_v$, respectively, if the particles evaporated.

depletion and conjecture that the electron depletion might be larger than shown in Fig. 4. If we assume that the amount of water vapor in the particles is equivalent to reasonable values of water vapor concentrations (let's say between 1 and 10 ppm$_v$) we find from Fig. 5 that the particles must have been very small (less than 3 nm radius) and the number density extremly large (more than 500,000 cm^{-3}). Such a huge amount of small particles has never been predicted or observed; on the other hand there is no direct theoretical or experimental evidence that such a population could not exist. We note that the tendency of many small particles at higher altitudes is in agreement with some theories about particle coagulation and sedimentation and their role in the creation of PMSE (Turco et al., 1982; Klostermeyer, 1997).

3.4. Case 3a. Flight DECB93

During this flight aerosol parameters have been determined from in situ measurements (Gumbel and Witt, 1998), however, no measurement of positive ion composition, and hence no recombination coefficient α is available. Therefore, we turn around the procedure used above. From the aerosol parameters we determine the recombination coefficient applying our model and draw conclusions on the positive ion composition. In Fig. 6 we reproduce the electron and ion number density measurements by the Faraday instrument and the positive ion probe (PIP), respectively, for this flight. The ion currents measured by PIP have been converted to number densities by normalizing the undisturbed flanks of the ion profile to the estimated undisturbed flanks of the electron number densities (dotted line). We take the particle radius and number density as estimated in Gumbel and Witt (1998): $r_A = 47$ nm and $N_A = 110$ cm^{-3}. In Fig. 7 we present model calculations of Δn_e and Δn_i as a function of Q and α using these values for r_A and N_A. In this figure we have marked combinations of Q and α leading to $\sqrt{Q/\alpha} = 100$ cm^{-3} which is a rough estimate of the undisturbed plasma density observed during this flight (see Fig. 7).

From Fig. 7 we see that the observed ion enhancement ($\Delta n_i \sim +100\%$) can only be explained with a recombination coefficient greater than 4×10^{-5} cm^3/s. Using the additional constraint of $\sqrt{Q/\alpha} = 100$ cm^{-3} leads to $\alpha = 4\times10^{-5}$ cm^3/s and $Q = 0.22$ cm^{-3}s^{-1}. This comparatively large value of α indicates that extremely heavy proton clusters (more than 7 ligands) must have been the dominant positive ions in the biteout layer during this flight (see R&L for more details).

4. Discussion and summary

The results of the model calculations for the four cases presented in Section 3 are summarized in Table 3. In the

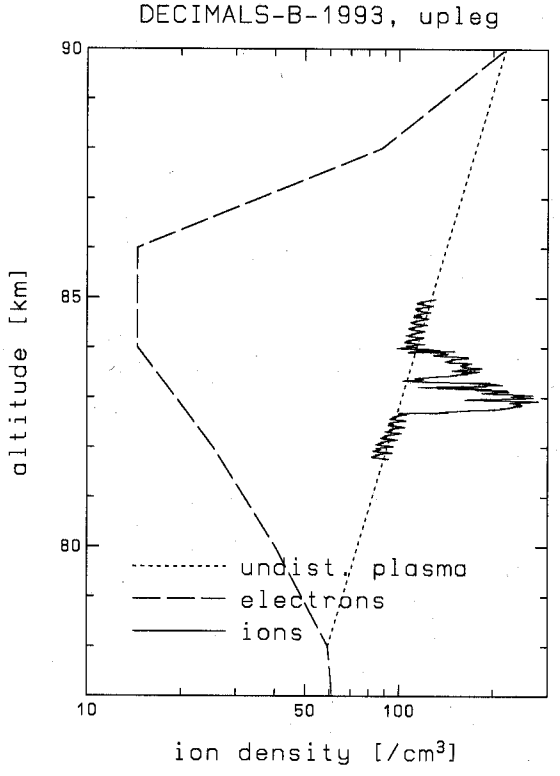

Fig. 6. Rocket borne measurements of positive ion densities (solid line) and electron densities (dashed line) during flight DECB93 (see Table 2). The dotted line indicates a rough estimate of the undisturbed electron density profile. Electron data are from Friedrich and Torkar (1995). The positive ion data have been provided by T.A. Blix and E.V. Thrane (personal communication).

three cases where an NLC was observed in the biteout region (flights S26/1, DECA93, and DECB93) the particle radii are 60, 32, and 47 nm, and the aerosol number densities are 180, 850, and 110 cm^{-3}, respectively. These values are in nice agreement with ground-based estimates of NLC particle parameters by lidars (e.g. von Cossart et al., 1999). We note that the amount of water in these particles corresponds to gas phase concentrations of $\sim$4–14 ppm_v, which is comparatively large compared to model values and the sparse experimental data on mean water vapor concentrations (Garcia and Solomon, 1994; Seele and Hartogh, 1999). These large values at NLC heights could indicate that water vapor has been scavenged over a larger horizontal and/or altitude range when the particles are sedimenting from the mesopause region at 88 km down to typical NLC altitudes, say at 82 km. This 'freeze-drying' effect has earlier been suggested in connection with NLC particle condensation, sedimentation and sublimation (Inhester et al., 1994; Turco et al., 1982).

In the PMSE case (flight JK72) the particles are much smaller (1 nm) and much more abundant (several 100,000 cm^{-3} up to 10 million, considering the uncertainties in the experimental data). These number densities are in fact much larger than the concentration of smoke particles predicted by the meteor ablation model of Hunten et al. (1980). This could imply that more numerous condensation particles, e.g. cluster ions, were present during this flight. This scenario is in agreement with model studies of particle condensation which suggest that ion nucleation leads to larger concentrations of small particles whereas dust nucleation leads to smaller concentrations of large particles (Turco et al., 1982). Which of the two mechanisms dominates is mainly controlled by the atmospheric temperature around the mesopause: Ion nucleation is preferred at very low temperatures whereas dust nucleation prevails at larger temperatures. Temperature measurements by the Lyman-α technique showed comparatively large values of $\sim$150 K (Johannessen et al., 1972). However, this technique is rather uncertain at mesopause altitudes. We note that many small particles are more difficult to detect by lidars than few large particles. A comparison of ground-based lidar observations of NLCs and in situ temperature measurements has indeed shown cases of very low mesopause temperatures with the confirmed absence of NLCs observed by the lidar (Lübken et al., 1996).

In Case 3a (studied in Section 3.4) the particle radius and number density are known from in situ measurements and we have applied our model to the electron and ion density disturbances to determine the recombination coefficient α and the ion/electron production rate Q. We arrive at a rather large value $\alpha \sim 4 \times 10^{-5}$ cm^3/s which implies the abundance of very heavy cluster ions with at least 7 water molecule ligands.

It is interesting to note that the atmospheric temperature plays a minor role in our model. Of course, a low enough temperature is crucial for the existence of ice particles at the summer mesopause region, however, the charging mechanism varies only slightly with electron and ion temperature. As mentioned earlier we have used the mean summer temperatures as published in Lübken (1999) in our model calculations.

In summary we have shown in this paper that the aerosol charging model is capable of explaining the existing data set on electron and ion depletions and enhancements, phenomena which are frequently observed in the vicinity of NLC and PMSE layers. From the model we derive particle parameters, such as radius r_A and number density N_A. We have demonstrated by studying various cases that the recombination coefficient α and the electron/ion production rate Q are crucial parameters in order to understand the effect of aerosol charging on the background plasma.

From the case studies presented above it is obvious that the influence of aerosols on the background plasma around the summer mesopause reveals a rather complex behaviour depending not only on the aerosol properties themselves but also on the ionospheric background conditions. In order to get a complete picture it is therefore highly desirable to

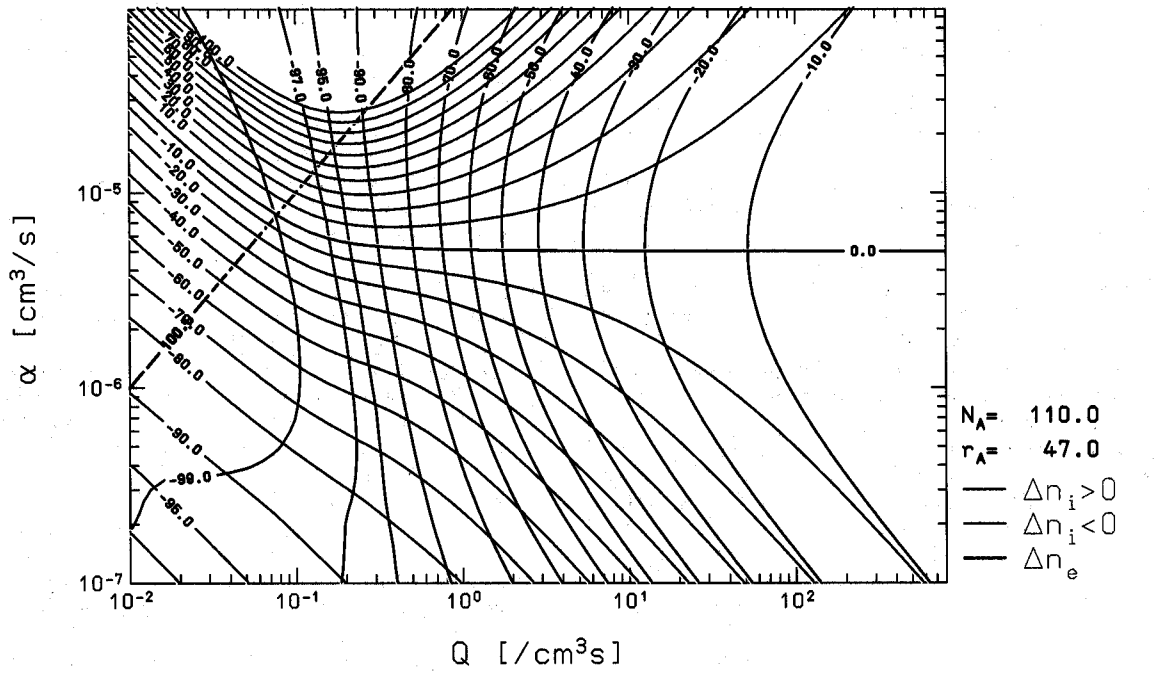

Fig. 7. Model calculations of Δn_e (blue lines) and Δn_i ($\Delta n_i > 0$, green, and $\Delta n_i < 0$, red lines) as a function of Q and α for flight DECB93. The black dashed line indicates combinations of Q and α leading to $\sqrt{Q/\alpha} = 100\ \mathrm{cm}^{-3}$ which is the undisturbed plasma density measured during this flight.

Table 3
Main results of the model calculations and parameters used in the model

	S26/1	DECA93	JK72	DECB93
r_A (nm)	60	32	1	47
N_A (cm^{-3})	180	850	10^7	110
Q ($cm^{-3}\ s^{-1}$)	1.35	0.006	383	0.22
α ($10^{-6}\ cm^{-3}\ s^{-1}$)	7.0	6.9	2.1	40.0
$c(H_2O)$ (ppm_v)	13.8	10.0	3.6	4.2

measure as many aerosol and ionospheric plasma parameters as possible.

Acknowledgements

We are grateful to T.A. Blix and E.V. Thrane for providing unpublished data from flight DECB93.

References

Balsiger, F., Kopp, E., Friedrich, M., Torkar, K.M., Wälchli, U., 1993. Small-scale structure of O_2^+ and proton hydrates in a noctilucent cloud and polar mesospheric summer echo of August 9/10 1991 above Kiruna. Geophysical Research Letters 20, 2315–2318.

Balsiger, F., Kopp, E., Friedrich, M., Torkar, K.M., Wälchli, U., Witt, G., 1996. Positive ion depletion in a noctilucent cloud. Geophysical Research Letters 23, 93–96.

Björn, L.G. et al., 1985. Heavy ionospheric ions in the formation process of noctilucent clouds. Journal of Geophysical Research 90, 7985–7998.

Blix, T.A., 1999. The importance of charged aerosols in the polar mesosphere in connection with noctilucent clouds and polar mesosphere summer echoes. Advances in Space Research 24 (12), 1645–1654.

Blix, T.A., Thrane, E., 1993. Noctilucent clouds and regions with polar mesospheric summer echoes studied by means of rocket-borne electron and ion DC-probes. Geophysical Research Letters 20, 2303–2306.

Cho, J.Y.N., Röttger, J., 1997. An updated review of polar mesosphere summer echoes: observation, theory, and their relationship to noctilucent clouds and subvisible aerosols. Journal of Geophysical Research 102, 2001–2020.

Friedrich, M., Torkar, K., 1995. An attempt to parameterize negative ions in the ionospheric D-region, Proceedings of the 12th ESA Symposium on European Rocket and Balloon Programmes and Related Research, Lillehammer, Norway (ESA SP), European Space Agency, Neuilly, France, 1995, pp. 257–261.

Friedrich, M., Torkar, K.M., Thrane, E., Blix, T., 1994. Common features of plasma density profiles during NLC. Advances in Space Research 14 (9), (9)161–(9)164.

Gadsden, M., Schröder, W., 1989. Noctilucent Clouds. Springer, New York.

Garcia, R.R., Solomon, S., 1994. A new numerical model of the middle atmosphere: 2. ozone and related species. Journal of Geophysical Research 99, 12,937–12,951.

Goldberg, R., Kopp, E., Witt, G., Swartz, W., 1993. An overview of NLC-91: a rocket/radar study of the polar summer mesosphere. Geophysical Research Letters 20, 2443–2446.

Gumbel, J., Witt, G., 1998. In situ measurements of the vertical structure of a noctilucent cloud. Geophysical Research Letters 25, 493–496.

Havnes, O., Trøim, J., Blix, T., Mortensen, W., Næsheim, L.I., Thrane, E., Tønnesen, T., 1996. First detection of charged dust particles in the Earth's mesosphere. Journal of Geophysical Research 101, 10,839–10,847.

Hunten, D., Turco, R., Toon, O.B., 1980. Smoke and dust particles of meteoric origin in the mesosphere and stratosphere. Journal of Atmospheric Science 37, 1342–1357.

Inhester, B., Klostermeyer, J., Lübken, F.-J., von Zahn, U., 1994. Evidence for ice clouds causing polar mesospheric summer echoes. Journal of Geophysical Research 99, 20,937–20,954.

Jensen, E., Thomas, G.E., 1991. Charging of mesospheric particles: implications of electron density and particle coagulation. Journal of Geophysical Research 96, 18,603–18,615.

Johannessen, A., Krankowsky, D., 1972. Positive ion composition measurement in the upper mesosphere and lower thermosphere at a high latitude during summer. Journal of Geophysical Research 77, 2888–2901.

Johannessen, A., Krankowsky, D., Arnold, F., Riedler, W., Friedrich, M., Folkestad, K., Skovli, G., Thrane, E.V., Troim, J., 1972. Detection of water cluster ions at the high latitude summer mesopause. Nature 235, 215–216.

Klostermeyer, J., 1997. A height- and time-dependent model of polar mesosphere summer echoes. Journal of Geophysical Research 102, 6715–6727.

Kopp, E., Eberhardt, P., Herrmann, U., Björn, L., 1985. Positive ion composition of the high latitude summer D-region with noctilucent clouds. Journal of Geophysical Research 90, 13,041–13,051.

Kopp, E., Ramseyer, H., Björn, L., 1984. Positive ion composition and electron density in a combined auroral and nlc event. Advances in Space Research 4, 157–161.

Lübken, F.-J., 1999. Thermal structure of the Arctic summer mesosphere. Journal of Geophysical Research 104, 9135–9149.

Lübken, F.-J., Rapp, M., Blix, M.T., Thrane, E., 1998. Microphysical and turbulent measurements of the Schmidt number in the vicinity of polar mesosphere summer echoes. Geophysical Research Letters 25, 893–896.

Lübken, F.-J., Fricke, K.-H., Langer, M., 1996. Noctilucent clouds and the thermal structure near the Arctic mesopause. Journal of Geophysical Research 101, 9489–9508.

Lübken, F.-J., Lehmacher, G., Blix, T., Hoppe, U.-P., Thrane, E., Cho, J., Swartz, W., 1993. First in-situ observations of neutral and plasma density fluctuations within a PMSE layer. Geophysical Research Letters 20, 2311–2314.

Mitra, A.P., 1981. Chemistry of middle atmospheric ionization—a review. Journal of Atmospheric and Terrestrial Physics 43, 737–752.

Parthasarathy, R., 1976. Mesopause dust as a sink for ionization. Journal of Geophysical Research 81, 2392–2396.

Pedersen, A., Troim, J., Kane, J., 1969. Rocket measurement showing removal of electrons above the mesopause in summer at high latitudes. Planetary and Space Science 18, 945–947.

Rapp, M., Lübken, F.-J., 1999. Modelling of positively charged aerosols in the polar summer mesopause region. Earth, Planets and Space 51, 799–807.

Rapp, M., Lübken, F.-J., 2001. Modelling of particle charging in the polar summer mesosphere: Part 1 — general results. Journal of Atmospheric and Solar Terrestrial Physics 63, 759–770.

Reid, G.C., 1990. Ice particles and electron "bite-outs" at the summer polar mesopause. Journal of Geophysical Research 95, 13,891–13,896.

Seele, C., Hartogh, P., 1999. Water vapor of the polar middle atmosphere: annual variation and summer mesosphere conditions as observed by ground-based microwave spectroscopy. Geophysical Research Letters 26, 1517–1520.

Thomas, L., Bowman, M.R., 1985. Model studies of the D-region negative-ion composition during day-time and night-time. Journal of Atmospheric and Terrestrial Physics 47, 547–556.

Turco, R.P., Toon, O.B., Whitten, R.C., Keesee, R.G., Hollenbach, D., 1982. Noctilucent clouds: simulation studies of their genesis, properties and global influences. Planetary Space Science 3, 1147–1181.

von Cossart, G., Fiedler, J., von Zahn, U., 1999. Size distributions of nlc particles as determined from 3-color observations of nlc by ground-based lidar. Geophysical Research Letters 26, 1513–1516.

Wälchli, U., Stegmann, J., Witt, J.Y.N.C.G., Miller, C.A., Kelley, M.C., Swartz, W.E., 1993. First height comparison of noctilucent clouds and simultaneous pmse. Geophysical Research Letters 20, 2845–2848.